A Novel Method for Studying Damage Rate Effects in Ion Bombarded Nickel

J.B. Whitley, P. Wilkes, and G.L. Kulcinski

June 1976

UWFDM-159

FUSION TECHNOLOGY INSTITUTE

UNIVERSITY OF WISCONSIN

MADISON WISCONSIN

A Novel Method for Studying Damage Rate Effects in Ion Bombarded Nickel

J.B. Whitley, P. Wilkes, and G.L. Kulcinski

Fusion Technology Institute
University of Wisconsin
1500 Engineering Drive
Madison, WI 53706

http://fti.neep.wisc.edu

June 1976

UWFDM-159

A Novel Method for Studying Damage Rate Effects in Ion Bombarded Nickel

J. B. Whitley
P. Wilkes
G. L. Kulcinski

June 1976

UWFDM-159

Introduction

Ever since the discovery of the problem of void swelling in structural materials, there has been an increasing effort to try and understand the dimensional behavior of metals under high temperature irradiations. In recent years, there has been an increased use of various techniques to try to simulate the neutron radiation environment by irradiating the sample with various charged particles. One powerful technique is to irradiate with high energy heavy ions, which increases the displacement rate by several orders of magnitude over neutron irradiations, and also gives an energy spectrum of the displaced atoms similar to that caused by high energy neutrons. One of the problems with this technique is the short range of the heavy ions into the sample, leading to uncertainties both in the quantitative analysis of the irradiated sample, and to uncertainties in the interpretation of the results. In certain cases, however, it it possible to prepare the irradiated sample in cross section such that the microstructure can be studied along the ion path. In this paper, the description and application of this technique to the study of high purity nickel irradiated with 19 MeV Cu ions will be discussed.

Experimental Methods

The material used in this study was MARZ grade nickel (>99.995%) obtained from Materials Research Corporation. The result of bulk analysis for several important impurities is given in Table I.

Table I

Material Analysis for MARZ Grade Nickel

Impurity Element	Content (wt-ppm)
O	<10.0
C	10.0
H	<1.0
N	<10.0
Fe	20.0
Cu	3.0
Ge	6.0
All Others	<5.0

After machining the foils into the proper shape for the irradiation, the samples were cleaned and given a recrystallization anneal at 1000°C for one hour in a helium atmosphere and furnace cooled. The samples were electropolished to give the cleanest possible surface prior to loading and irradiated in a high temperature, ultra-high vacuum target chamber which has been described elsewhere.[1]

All samples were irradiated at a temperature of 525°C with 19 MeV Cu ions to fluences up to 10^{16} ions/cm^2. The damage energy deposition as a function of depth was determined using the E-DEP-1 code of Manning and Mueller.[2] The threshold displacement energy was taken as 24 eV,[3] with the dpa values calculated using the modified Kinchin and Pease[4] formula as follows:

$$n_d = \frac{\beta\nu(E)}{2E_d} ,$$

where n_d is the number of displacements, $\nu(E)$ the E-DEP-1 damage energy result, β a connection factor taken as 0.8, and E_d the effective displacement energy taken as 5/3 the threshold displacement energy. The result of this calculation is shown in Figure 1 for 19 MeV Cu ions incident on a nickel target. Note that the right hand axis gives the dpa rates corresponding to the ion flux used in this experiment. Also shown is the relative range distribution of the implanted Cu ions.

After irradiation, the samples were prepared in cross sections using a technique similar to that used by Spurling and Rhodes on proton irradiated stainless steel.[5] In our procedure, the sample is first given an activation treatment in a solution of Wood's nickel by making the sample anodic for ~20 seconds at a current density of 25 mA/cm^2.[6] This step is necessary to remove the metal oxide layer and assure a good bond. The amount of material removed in this process has been estimated to be <500 Å by interference microscopy. After activation, the current is reversed in this same solution and a thin nickel strike is applied. The sample is then transferred directly to a high chlorine nickel plating solution containing 150 g $NiSO_4$, 150 g $NiCl_2$ and 50 g boric acid in 1000 ml H_2O. Plating for ~24 hours in this solution at 50°C and a current density of ~300 mA/cm^2 will result in a final thickness of plated nickel greater than 2 mm. This sample is then mounted in resin and sliced in cross section using a low speed diamond saw. 3 mm discs are then removed from these slices and thinned for TEM in a twin jet electropolishing unit.

Analysis was carried out on a JEM 100B electron microscope operated at 125 kV. The depth distribution of void data was determined by dividing the micrographs into regions .25 microns wide parallel to the front surface. Foil

thicknesses were determined by stereo microscopy and the void data reduced in a manner similar to Ryan.[7]

Experiment Results

Voids were observed to form quite readily after the 19 MeV Cu irradiations at 525°C, even without prior He injection. A typical micrograph of the full damage region of a sample irradiated to a fluence of 10^{16} ion/cm^2 is shown in Figure 2. At the left hand side, the foil surface is clearly visible and well defined. There is a definite denuded region near the front surface, with no voids observed closer than ~1000 Å to the surface, followed by an additional 1500 Å region of inhibited void formation. Over the next micron of depth, both the void size and void density remain approximately constant, and then the void density quickly rises while the void size drops. Near the end of range, the void density drops and reaches zero at no clearly definable boundary. In all samples, voids were observed at depths of 3.6 to 3.75 μ, depths which are beyond that predicted for the ion range in Figure 1 by about 15%.

A side by side comparison of a limited dose scan carried out at 525°C is shown in Figure 3. Note that the void structure in the end of range region developed relatively slowly, with the low dose sample showing only a few voids at depths of 3.6 microns, while the higher dose samples have a much better defined void cut-off with many voids at 3.6 to 3.7 microns. Otherwise, these samples follow the trend expected at low doses of increasing void density and size with increasing dose.

As was stated previously, the voids were analysed by dividing the damage region into depth intervals of .25 micron. The variation of void density with depth is shown in Figure 4, where the data points are placed in the center of their respective depth intervals. Note that the general shape of the density curve follows the damage curve of Figure 1 reasonably well. Note also that the density curve of

the two larger dose samples seem, within experimental error, to have saturated. This indicates that the final void density is determined by the dose rate, and not the total dose.

Due to difficulties in microscopy, void size and swelling data were not determined for the low dose sample. However, these were measured for the two high dose samples, and a complete summary of this data is shown in Table II. The average void size is plotted as a function of depth in Figure 5. Since the void densities of these two samples are about equal, implying that nucleation has essentially ceased, the rate of change in void sizes in these samples will be the result of void growth alone. As can be seen, the void growth is suppressed near the end of range, and since the total dpa level is about six times greater in this region than at a depth of one micron, the void growth rate per dpa near the peak damage region is approximately a factor of 8 less than that at a depth of one micron. The peak in the void size curve at ~1 micron for the high dose sample is not understood, but may be due to the slight increase in dose in this region of approximately constant void density.

The swelling versus depth curves of Figure 6 show quite clearly the suppression of void growth in the peak damage region. Apparently the swelling profile, which develops in a fairly uniform manner during the nucleation stage, quickly changes character during growth. This change is shown more clearly in Figure 7, where the swelling data of Figure 6 are shown plotted as a function of the dpa level for that particular point. This plot, which only includes the points at depths less than the peak in the damage curve, shows that those points at depths greater than the peak in the swelling curve (indicated by filled symbols) do not correlate with a simple functional dependence of swelling on dose as do the other points. There are several possible reasons for this behavior. First of all, in a region of rapidly varying dose rates, one could expect large changes in the kinetic

behavior of void growth . A measure of this effect is given by the effective temperature shift, and if the shift is calculated using the model of Brailsford and Bullough,[8] a shift of ~40°C is found between one micron and the peak damage regions. Since 525°C is below the peak swelling temperature, then a steep gradient in the swelling vs. temperature curve could lead to a suppression of swelling in the peak region. Having a lower "effective" temperature in the peak region is consistent with the observed higher void density and smaller void size in this region. However, due to the variation in dose over this region, the swelling vs. temperature gradient would have to be very steep to actually reduce the swelling.

Another possible explanation is the effect of the implanted copper ions. If one assumes that the copper ions do not diffuse significantly from their final positions, then the final copper concentrations near the end of range approach several tenths of one percent. If the effect of copper atoms is to reduce the void growth rate by interacting with point defects, then the behavior of Figure 5 and 6 might be expected.

Discussion

Since so much data is extracted by the cross sectioning technique, it is useful to discuss the experimental conditions which do and do not vary with depth. First, those parameters such as sample heat treatment history, handling, irradiation temperature, ion flux and total fluence are all identical for a given sample. The features that vary with depth include total dose, dose rate, PKA distance from the front surface, impurity levels, internally generated stress levels, etc. Since so many parameters are rapidly changing with depth, one is restricted to analyse the results in a fairly narrow depth interval to avoid smearing out changes. This leads to the primary problem with the analysis by cross section technique, that of statistics. As is shown in Table II, the total number

Table II

19 MeV Cu on Ni

525°C

ion Dose (cm^{-2})	Depth (μ)	dpa	n*	$Nx10^{15}(cm^{-3})$	$\bar{d}$(Å)	σ(Å)**	ΔV/V(%)
1×10^{16}	.125	1.3	29	.52	335	54	1.13
	.375	1.5	82	.75	301	54	1.18
	.625	1.8	51	.50	338	70	1.10
	.875	2.0	41	.42	392	60	1.46
	1.125	2.4	56	.94	373	67	2.04
	1.375	3.0	64	1.20	330	59	2.51
	1.625	4.0	78	1.80	284	56	2.43
	1.875	4.9	81	2.10	300	70	3.16
	2.125	8.0	142	2.7	261	49	2.81
	2.375	12.0	210	3.9	225	49	2.63
	2.625	7.5	242	4.4	206	40	2.25
	2.875	1.0	138	2.55	234	44	1.90
	3.125	0	52	1.25	261	41	1.25
	3.375	0	19	.60	189	33	0.26
5×10^{5}	.125	.65	19	.16	317	36	.28
	.375	.75	58	.46	310	52	.78
	.625	.90	81	.65	280	52	.81
	.875	1.0	111	.89	253	42	.82
	1.125	1.2	114	.91	252	41	.82
	1.375	1.50	136	1.04	259	47	1.04
	1.625	2.0	189	1.5	236	43	1.14
	1.875	2.45	234	1.9	215	36	1.05
	2.125	4.0	337	2.7	203	38	1.31
	2.375	6.0	412	3.3	197	37	1.46
	2.625	3.7	557	4.5	181	37	1.56
	2.875	0.5	463	4.0	183	32	1.39
	3.125	0	184	1.5	220	36	.89
	3.375	0	64	.51	242	27	.39
	3.625	0	43	.52	134	37	.08

* n = total number of voids in the depth interval.

** See Reference 7

of voids counted in the low density region is very small, leading to significant statistical uncertainty. In most cases, however, this statistical error is less than 10%, and hence is acceptable. The relative error between intervals as a given sample is much smaller than the magnitude of the absolute error since the analysis is carried out on adjacent micrographs, leading to a reduction in such things as the foil thickness and magnification errors.

The generally good agreement between the peak in the void density and the peak in the dpa curve seems to indicate that the energy loss calculated by the E-DEP-1 code is not in great error. However, the observation of voids at greater depths than predicted would be consistent with either the electronic energy being overestimated, such as suggested by Narayan and Oen,[9] or that the magnitude of the range straggling has been underestimated, or both. The diffusion of point defects away from the peak damage region would give an additional effect, but this would be expected to give a small contribution after the irradiation microstructure is established.

The micrograph in Figure 8 shows the denuded region at the front surface very clearly. As was stated earlier, the amount of surface removed in the preparation is less than 500 Å, so the denuded region is from 1000-1500 Å. There is a slight increase in the size of the voids adjacent to the denuded region, but it is not significant, and not as large as differences observed at the edge of grain boundary denuded regions. The amount of denuding at the front surface was approximately the same as that observed at grain boundaries, but due to grain boundary migration and the small number of grain boundary areas observed, a quantitative comparison was not possible.

The voids observed were all octahedral with {100} truncation. The amount of truncation was observed to increase with depth. This would be expected from energy considerations, with the voids in the higher dose rate region deviating farther from their equilibrium shape.

A comparison of the results of this work with some previous heavy ion irradiations is shown in Figure 9. The results shown from this study are those indicated by the line of Figure 7 after the data were reduced to a linear plot of swelling vs. dpa. In this study, the displacement rate is $\sim 2 \times 10^{-4}$ dpa/sec, while Ryan's work[10] was at $\sim 3 \times 10^{-3}$ dpa/sec and Kulcinski et al.[11] at $\sim 10^{-2}$ dpa/sec. Thus, these results are consistent with 525°C being below the maximum swelling temperature and hence a lower displacement rate leading to greater swelling at a given temperature.

The dislocation density showed a significant variation with depth as is shown in Figure 10. The structure consisted of well developed dislocation cells with the tangled cell walls often connecting voids. Very few loops were observed. The dislocation structure well beyond the damaged region is shown in Figure 11b, with Figure 11a showing the as-annealed structure. The dislocation cell structure is presumably due to the irradiation and not from the preparation procedure since many unirradiated samples were prepared in cross section and the damage introduced was minimal. It is probable that this structure is a consequence of the relief of swelling stresses with considerable simultaneous dislocation climb and glide. A definite answer to this question must await further studies.

Acknowledgement

This research was supported by grants from the Energy Research and Development Administration and the Wisconsin Electric Utilities Research Foundation.

References

(1) R. G. Lott and H. V. Smith, Jr., "A High Temperature, High Vacuum Facility for Heavy Ion Simulation Studies," in Experimental Methods for Charged-Particle Irradiations, Gatlinburg, Tenn., 1975, CONF-750947, p. 82.

(2) I. Manning and G. P. Mueller, Computer Physics Communications 7, (1974) pp. 85-94.

(3) P. G. Lucasson and R. M. Walker, Phys. Rev. 127, p. 485 (1962).

(4) J. E. Westmoreland, J. A. Sprague, F. A. Smidt, Jr., and P. R. Malnberg, Rad. Effects 26, pp. 1-16 (1975).

(5) R. A. Spurling and C. G., Jnl. Nuc. Mat. 44 (1972) pp. 341-344.

(6) T. M. Rodgers, Handbook of Practical Electroplating p. 225. Macmillian Co., New York (1959).

(7) T. D. Ryan, Heavy Ion Induced Void Formation in Nickel, Ph.D. Thesis, Univ. of Mich., (1975) p. 64.

(8) A. D. Brailsford and R. Bullough, Jnl. Nuc. Mat. 49 (1972) p. 121.

(9) J. Narayan and O. S. Oen, ORNL Progress Report, (1975) p. 78, ORNL-5135.

(10) T. D. Ryan, Ref. 7, p. 94.

(11) G. L. Kulcinski, J. L. Brimhall, H. E. Kissinger, Radiation Induced Voids in Metals, Albany, New York, 1972, CONF-710601, p. 449.

Figure Captions

Fig. 1 - The displacement damage curve for 19 MeV Cu ions incident on a nickel target as calculated by the Manning & Mueller E-DEP-1 code.

Fig. 2 - The variation in void microstructure with depth. The peak calculated damage level was ~12 dpa at a depth of 2.4 microns.

Fig. 3 - A comparison of the damage region from three different dose levels, all irradiated at 525°C.

Fig. 4 - The variation in void density with depth for the three different doses. The data points lie in the center at their respective intervals.

Fig. 5 - The void size data for the two higher dose samples.

Fig. 6 - The swelling vs depth curves from the two high dose samples showing the strong reduction in the swelling rate near the end of range.

Fig. 7 - The swelling vs dpa obtained from Table II is shown here, with the square symbols corresponding to the $1 \times 10^{16} cm^{-2}$ dose sample, and the circles to the $5 \times 10^{15} cm^{-2}$ dose sample. The filled symbols are those values taken at depths of greater than 2 microns.

Fig. 8 - Detail of the denuded region at the foil surface.

Fig. 9 - A comparison of studies on undoped, heavy ion irradiated nickel. The results from this study were taken as the line drawn in Fig. 7.

Fig. 10 - The variation in dislocation structure with depth.

Fig. 11 - A view of the dislocation structure beyond the irradiated region.

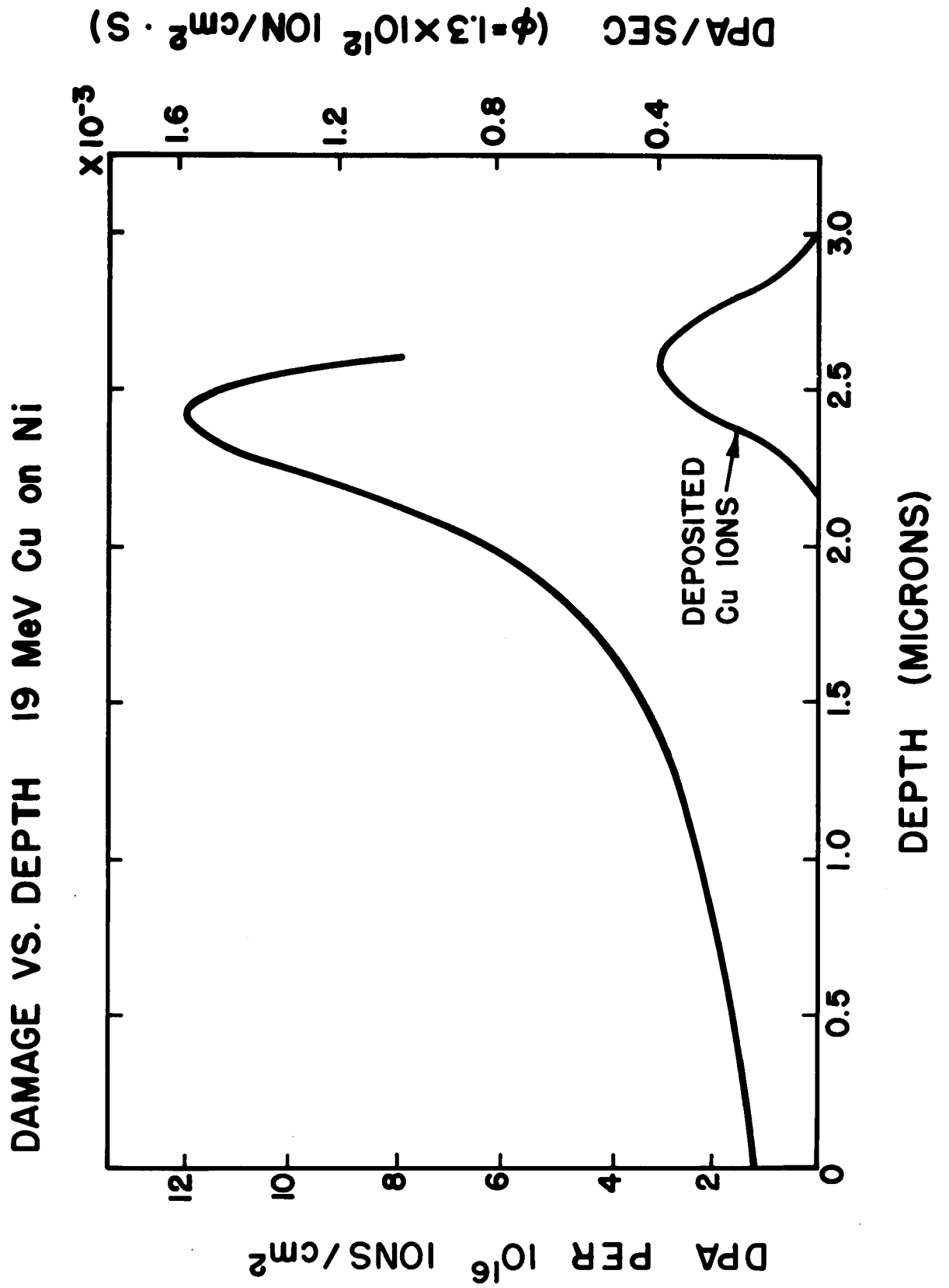
DAMAGE VS. DEPTH 19 MeV Cu on Ni
DPA PER 10^{16} IONS/cm^2
DEPTH (MICRONS)
DPA/SEC (ϕ=1.3×10^{12} ION/cm^2 · S)
×10^{-3}
DEPOSITED Cu IONS
0
0.5
1.0
1.5
2.0
2.5
3.0
2
4
6
8
10
12
0.4
0.8
1.2
1.6

FIGURE 1

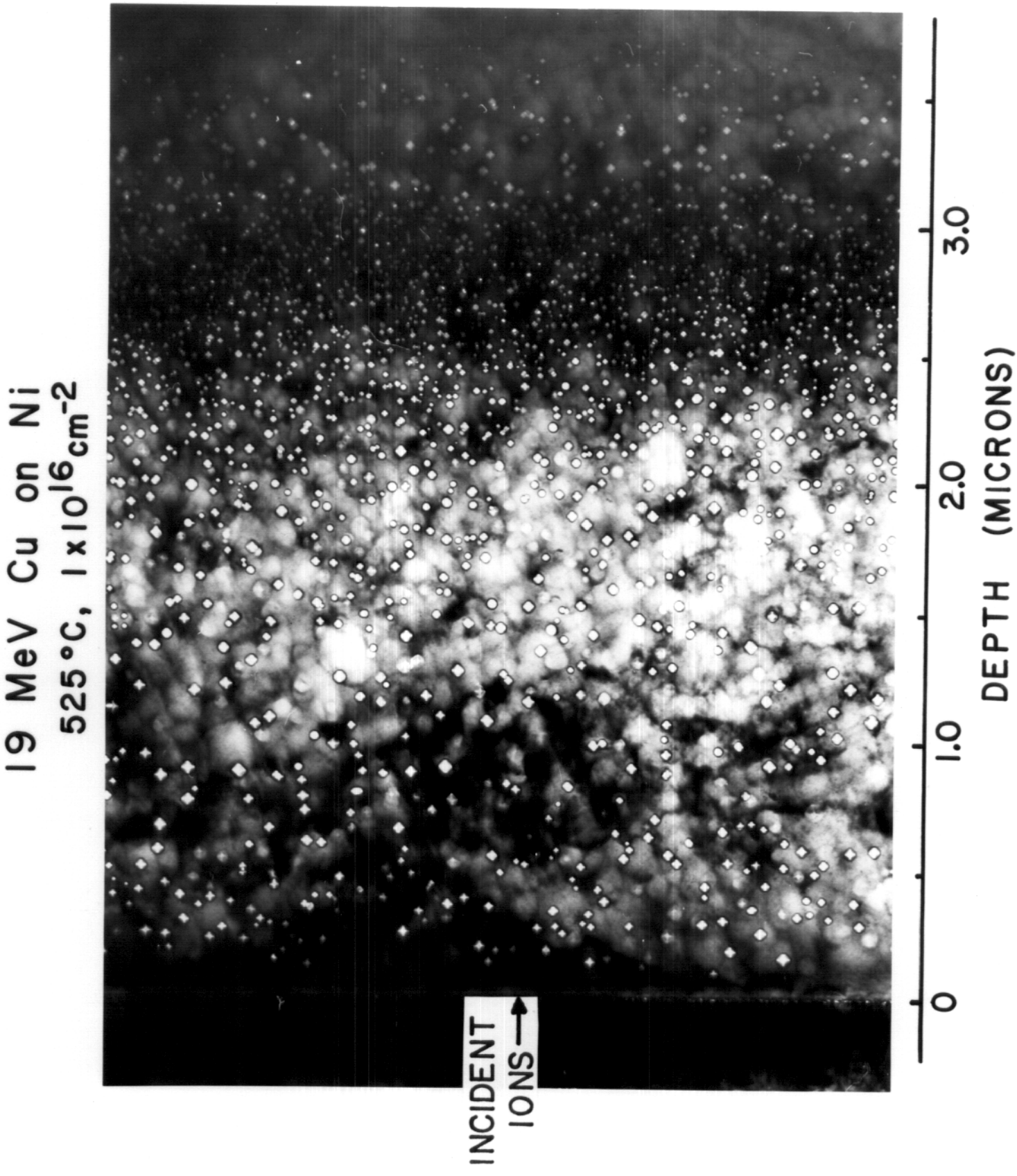
19 MeV Cu on Ni
525°C, 1x10^16 cm^-2
INCIDENT IONS
0
1.0
2.0
3.0
DEPTH (MICRONS)

FIGURE 2

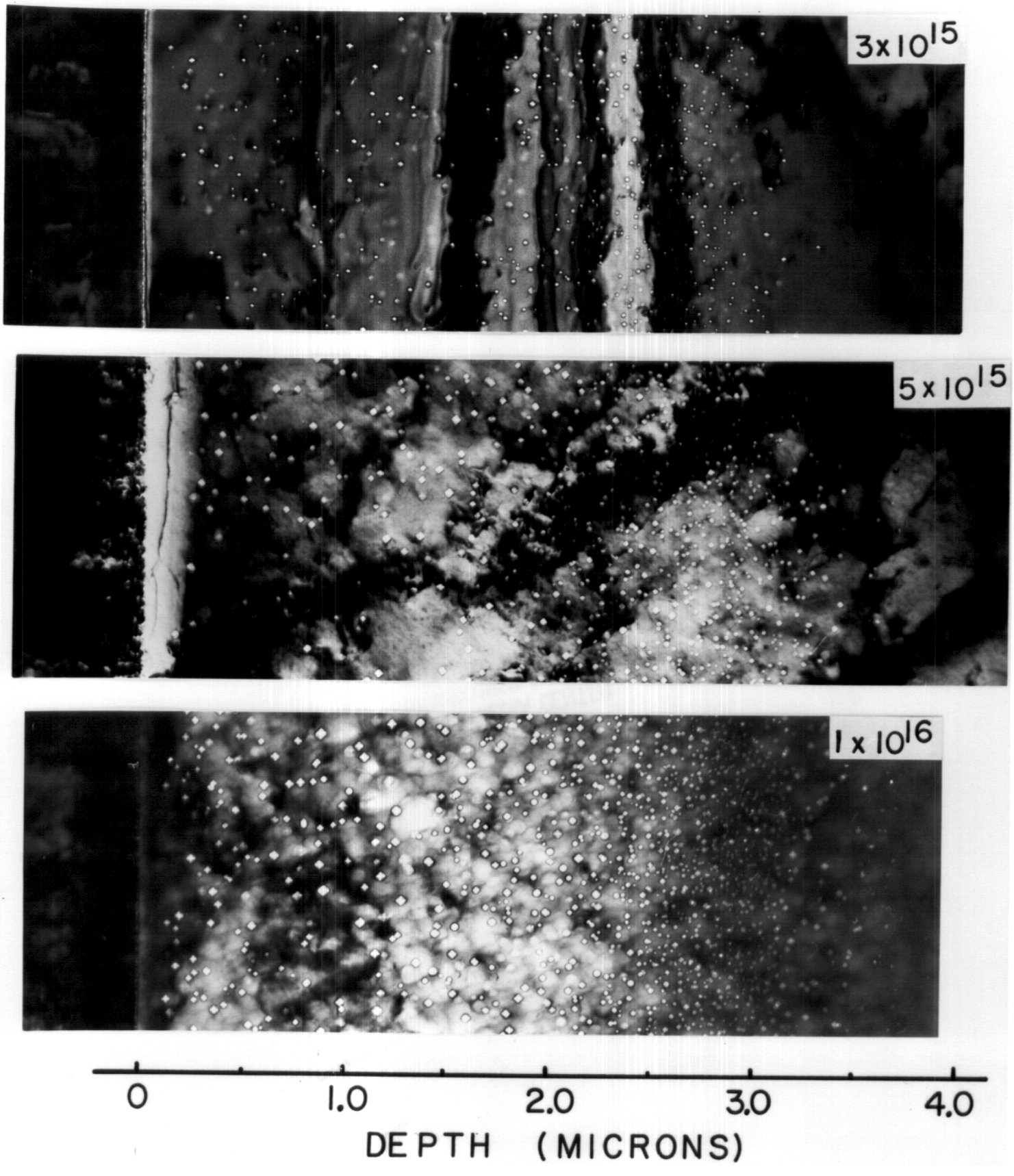
19 MeV Cu on Ni
525 °C
3x10^15
5x10^15
1x10^16
0
1.0
2.0
3.0
4.0
DEPTH (MICRONS)

FIGURE 3

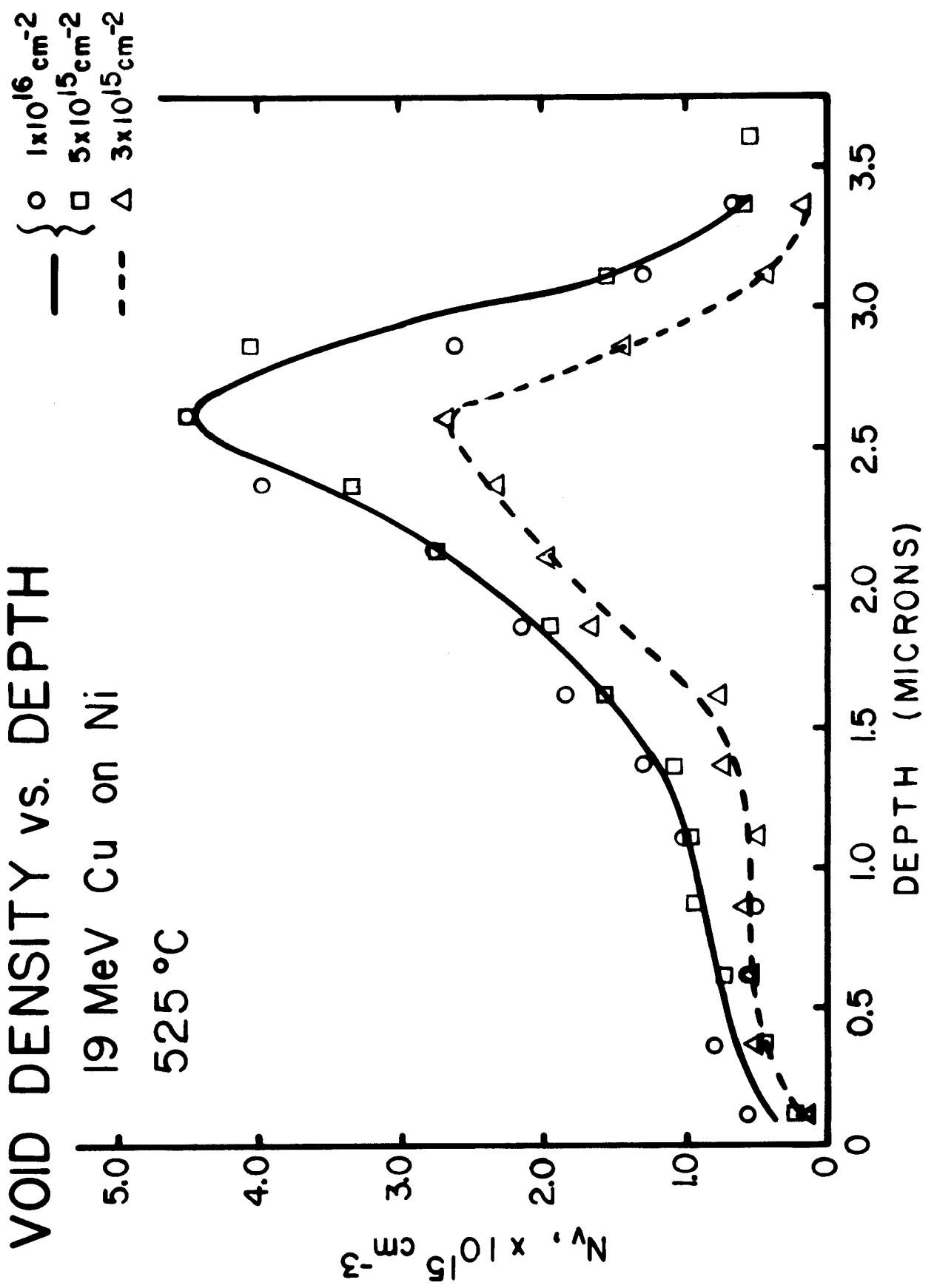
VOID DENSITY vs. DEPTH
19 MeV Cu on Ni
525 °C
o 1x10^16 cm^-2
□ 5x10^15 cm^-2
Δ 3x10^15 cm^-2
N_v, x 10^15 cm^-3
DEPTH (MICRONS)
0
0.5
1.0
1.5
2.0
2.5
3.0
3.5
1.0
2.0
3.0
4.0
5.0

FIGURE 4

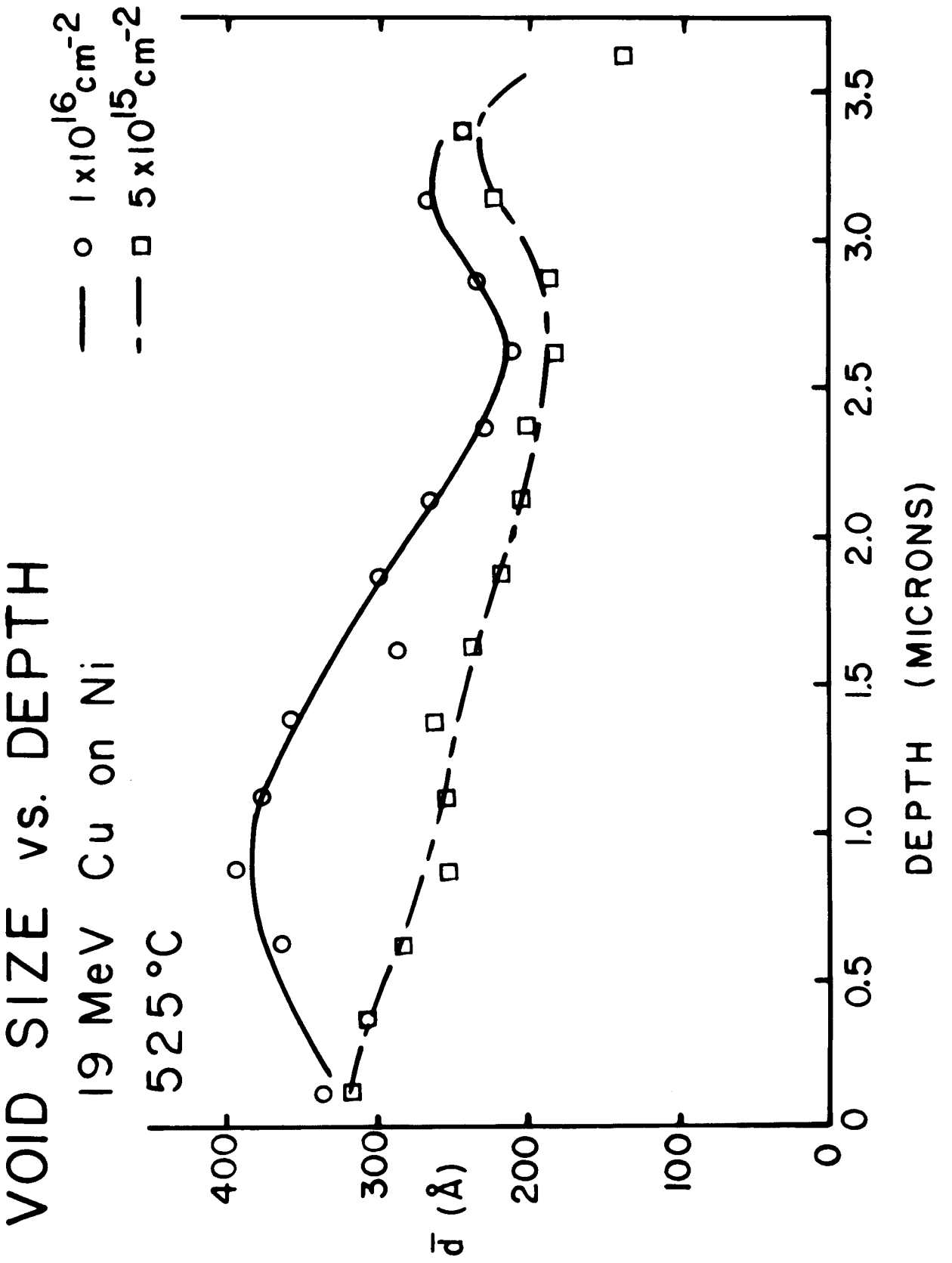
VOID SIZE vs. DEPTH
19 MeV Cu on Ni
525 °C
o 1x10^16 cm^-2
□ 5x10^15 cm^-2
d̄ (Å)
400
300
200
100
0
0
0.5
1.0
1.5
2.0
2.5
3.0
3.5
DEPTH (MICRONS)

FIGURE 5

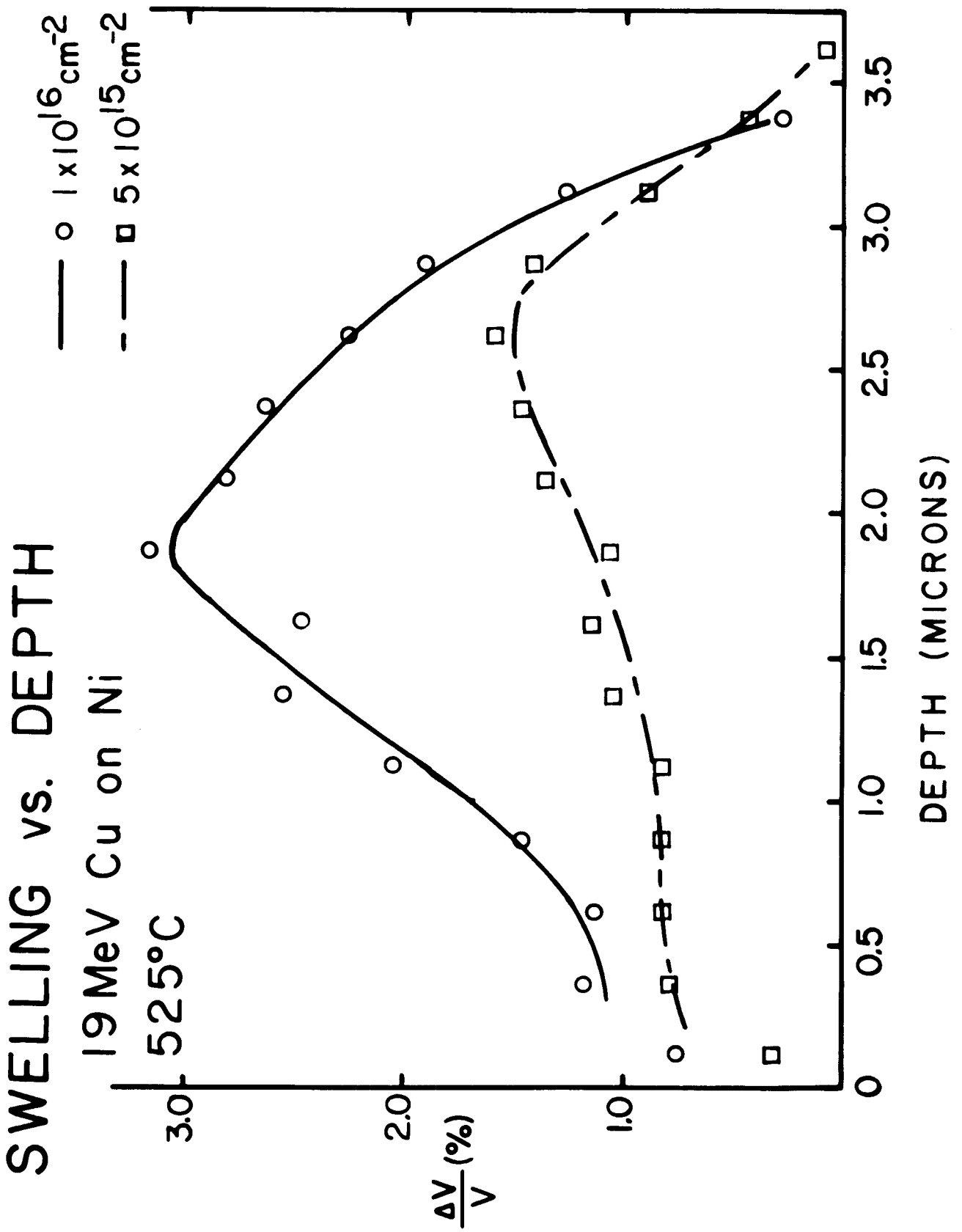
SWELLING vs. DEPTH
19 MeV Cu on Ni
525°C
o 1 x 10^16 cm^-2
□ 5 x 10^15 cm^-2
ΔV/V (%)
3.0
2.0
1.0
0
0.5
1.0
1.5
2.0
2.5
3.0
3.5
DEPTH (MICRONS)

FIGURE 6

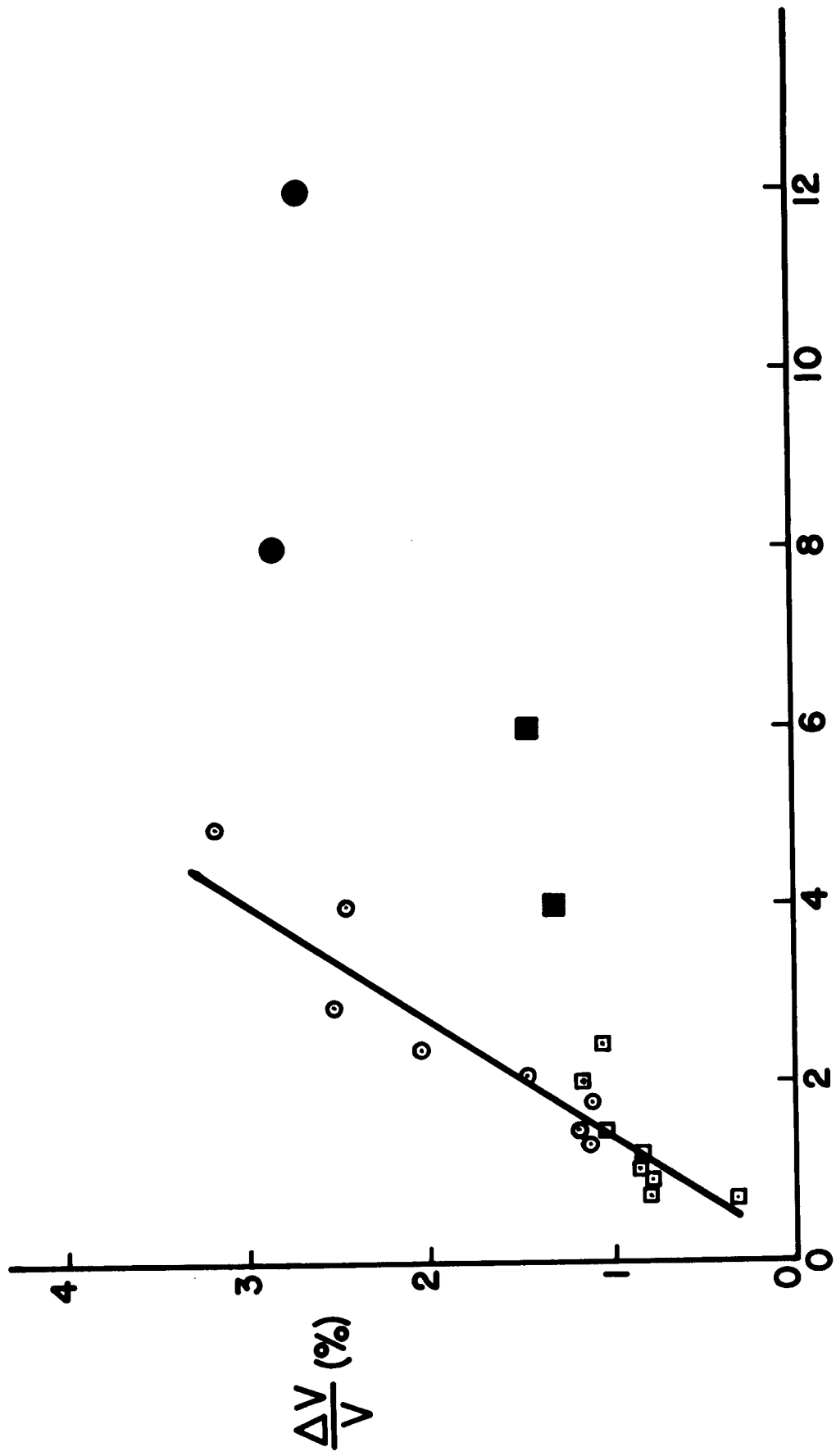

FIGURE 7

FIGURE 8

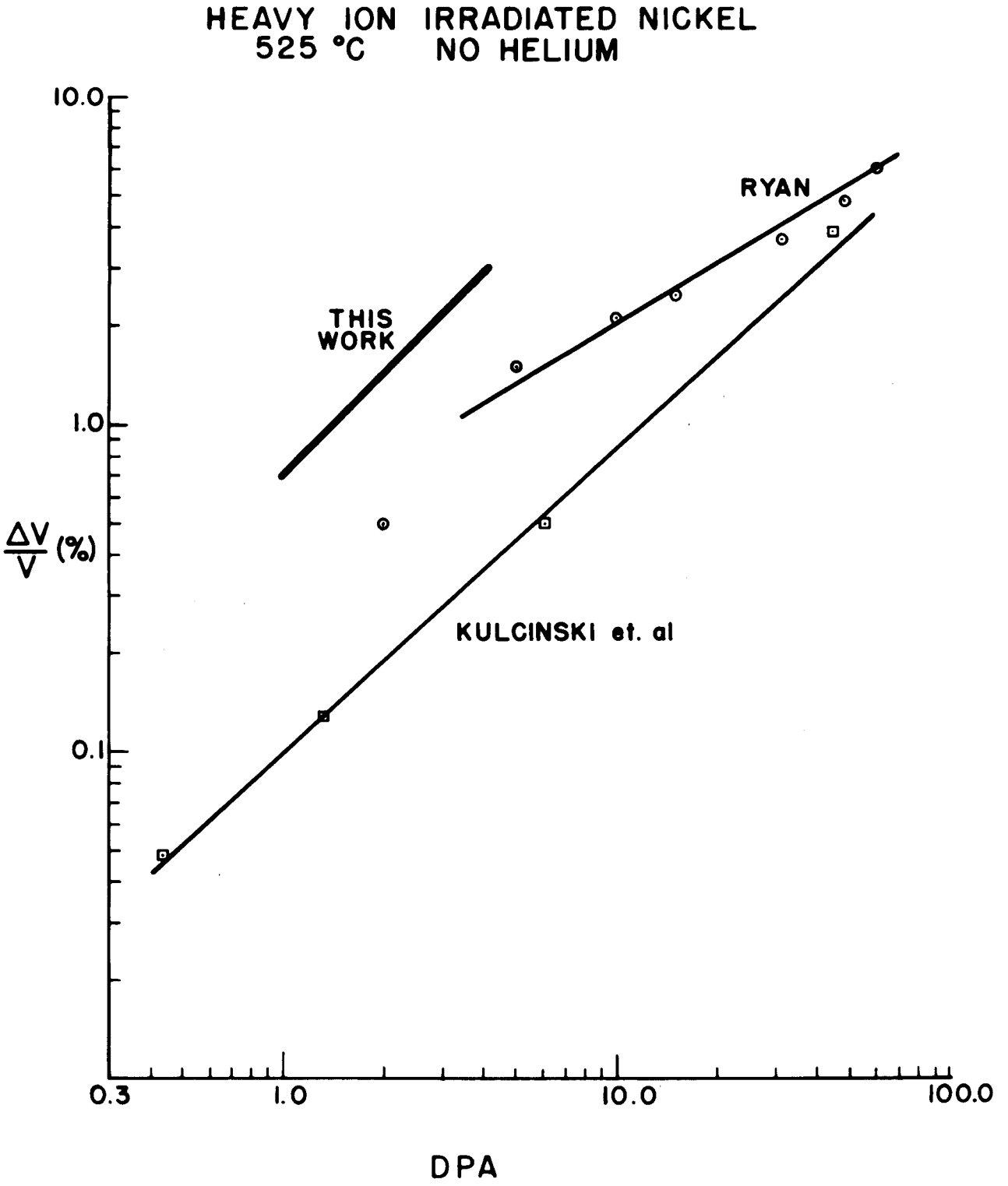
HEAVY ION IRRADIATED NICKEL
525 °C NO HELIUM
10.0
1.0
0.1
ΔV/V (%)
RYAN
THIS WORK
KULCINSKI et. al
0.3
1.0
10.0
100.0
DPA

FIGURE 9

FIGURE 10

DISLOCATION STRUCTURE IN UNIRRADIATED REGIONS

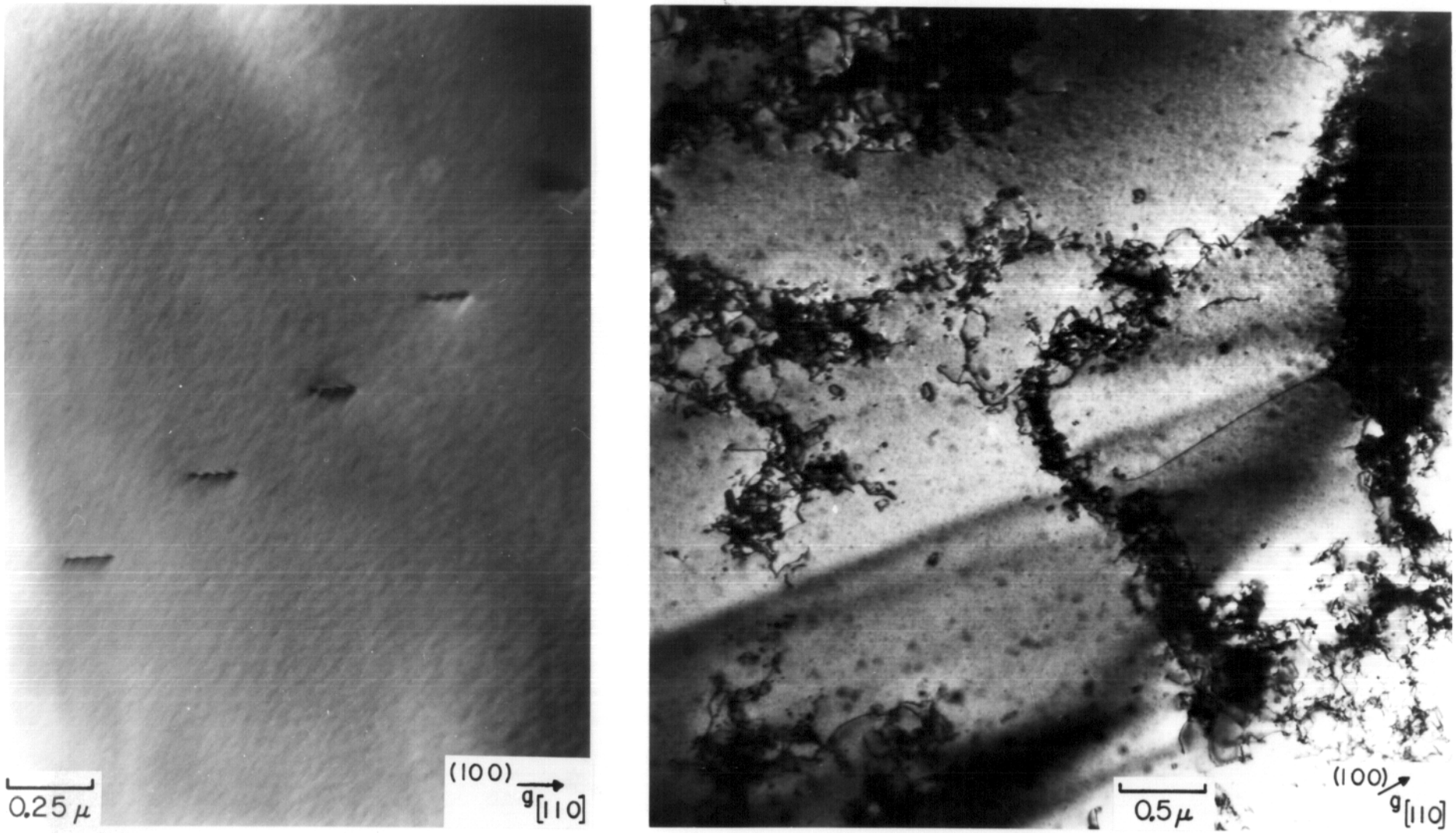

a.) CONTROL

b.) REGION ~30 μ BEYOND AN IRRADIATED ZONE

FIGURE 11